Published in final edited form as:
Neuroscience. 2010 September 29; 170(1): 178–188. doi:10.1016/j.neuroscience.2010.06.017.

Ultrastructural Characterization of the Optic Pathway in a Mouse Model of Neurofibromatosis-1 Optic Glioma

K-.Y. KIM[a], **W-. K. JU**[b], **B. HEGEDUS**[c], **D. H. GUTMANN**[c], and **M. H. ELLISMAN**[a,*]

[a]Center for Research in Biological Systems, National Center for Microscopy and Imaging Research and Department of Neurosciences, University of California San Diego School of Medicine, La Jolla, CA 92037

[b]The Sophie and Arthur Optic Nerve Laboratory, Hamilton Glaucoma Center, University of California San Diego, La Jolla, CA 92037

[c]Department of Neurology, Washington University School of Medicine, St. Louis, MO 63110

Abstract

The purpose of this study was to investigate the progression of changes in retinal ganglion cells and optic nerve glia in neurofibromatosis-1 (NF1) genetically-engineered mice with optic glioma. Optic glioma tumors were generated in *Nf1*+/− mice lacking *Nf1* expression in GFAP+ cells (astrocytes). Standard immunohistochemistry methods were employed to identify astrocytes (GFAP, S100β), proliferating progenitor cells (sox2, nestin), microglia (Iba1), endothelial cells (CD31) and retinal ganglion cell (RGC) axons (Neurofilament 68k) in *Nf1*+/−, *Nf1*^{GFAP}CKO (wild-type mice with *Nf1* loss in glial cells), and *Nf1*+/−^{GFAP}CKO (*Nf1*+/− mice with *Nf1* loss in glial cells) mice. Ultrastructural changes in the optic chiasm and nerve were assessed by electron microscopy (EM). RGC were counted in whole retina preparations using high-resolution, mosaic confocal microscopy following their delineation by retrograde FluoroGold labeling. We found that only *Nf1*+/−^{GFAP}CKO mice exhibited gross pre-chiasmatic optic nerve and chiasm enlargements containing aggregated GFAP+/nestin+ and S100β+/sox2+ cells (neoplastic glia) as well as increased numbers of blood vessels and microglia. Optic gliomas in *Nf1*+/−^{GFAP}CKO mice contained axon fiber irregularities and multilamellar bodies of degenerated myelin. EM and EM tomographic analyses showed increased glial disorganization, disoriented axonal projections, profiles of degenerating myelin and structural alterations at nodes of Ranvier. Lastly, we found reduced RGC numbers in *Nf1*+/−^{GFAP}CKO mice, supporting a model in which the combination of optic nerve *Nf1* heterozygosity and glial cell *Nf1* loss results in disrupted axonal-glial relationships, subsequently culminating in the degeneration of optic nerve axons and loss of their parent RGC neurons.

Keywords

neurofibromatosis-1; optic glioma; astrocyte; retinal ganglion cell; microglial cell; electron microscope tomography

Correspondence to: Mark H. Ellisman, Ph.D. Phone: 858 534-2251; Fax: 858 534-7497 mellisman@ucsd.edu.

Introduction

Neurofibromatosis type 1 (NF1) is a common autosomal dominant disorder that affects 1 in 3,000 people worldwide (Friedman, 1999). Individuals with NF1 are prone to the development of both benign and malignant nervous system tumors, including Schwann cell tumors (neurofibromas) and astrocytomas. The most common brain tumor seen in children with NF1 is a low-grade glial neoplasm that forms along the optic pathway (optic pathway glioma; OPG) (Listernick et al., 1989, Listernick et al., 1994). One-third to one-half of these tumors causes clinical symptoms, including visual loss and hypothalamic dysfunction (Listernick et al., 1994, Listernick et al., 1995, Balcer et al., 2001, Listernick et al., 2004, Thiagalingam et al., 2004). However, following treatment, few children with symptomatic optic gliomas have significant improvements in their vision (Dalla Via et al., 2007), suggesting that irreversible axonal dysfunction accompanies optic glioma formation and growth.

Individuals with NF1 are born with one functional and one mutated *NF1* allele in every cell of their body: Tumor formation ensues only after the one remaining functional *NF1* gene undergoes somatic mutation. In this regard, the brains of children with NF1 are composed of *NF1*+/− cells while the glial cells in the optic gliomas completely lack *NF1* gene expression. To model optic gliomas in genetically-engineered mice, we previously developed *Nf1*+/− mice lacking *Nf1* protein (neurofibromin) expression in astrocytes (Bajenaru et al., 2003). These *Nf1*+/−^{GFAP}CKO mice develop optic nerve and chiasm low-grade astrocytomas that share many features of human NF1-associated optic gliomas, and have been extensively employed for basic science and preclinical translational science studies (Bajenaru et al., 2005, Daginakatte and Gutmann, 2007, Warrington et al., 2007, Hegedus et al., 2008, Hegedus et al., 2009).

Children with NF1-associated OPG may initially present loss of visual acuity, reduced color vision, abnormalities in visual evoked potentials, or optic nerve atrophy (Listernick et al., 1997, Wolsey et al., 2006). These clinical findings suggest damage to optic nerve axons: Axonal injury is known to lead to changes in retinal ganglion cell (RGC) function, eventually resulting in their death (Quigley et al., 1995, Levin and Gordon, 2002). Based on previous studies demonstrating that perturbations in the periaxonal environment can affect rapid anterograde and retrograde axonal transport in optic nerve axons, leading to axonal atrophy and RGC loss (Anderson and Hendrickson, 1974, Minckler et al., 1977, Quigley et al., 1979, Johnson et al., 2000, Pease et al., 2000, Quigley et al., 2000, Levin and Gordon, 2002), we employed the *Nf1*+/−^{GFAP}CKO preclinical optic glioma mouse model to characterize the relationship between neoplastic astrocytes and neurons. Using a combination of light and electron microscopy approaches, we demonstrate ultrastructural features of optic glioma-associated axonopathy, destabilization of axon-glial interactions, and RGC loss.

EXPERIMENTAL PROCEDURES

Animals

All procedures concerning animals were in accordance with the ARVO Statement for the Use of Animals in Ophthalmic and Vision Research and under protocols approved by institutional IACUC committees at Washington University and the University of California-San Diego. *Nf1*^{GFAP}CKO and *Nf1*+/−^{GFAP}CKO mice were generated as previously described (Bajenaru et al., 2002, Bajenaru et al., 2003). Age-matched control animals were *Nf1*$^{flox/flox}$ (equivalent to wild-type) and *Nf1*+ mice. All mice were 9 months of age, maintained on a C57BL/6 background, housed in covered cages, fed with a standard rodent diet ad libitum, and kept on a 12-hour light/12-hour dark cycle.

Immunohistochemistry

Mice were transcardially perfused with oxygenated Ringer's solution at 37°C, followed by 4% paraformaldehyde (PFA, Sigma, St. Louis, MO) in phosphate-buffered saline (PBS) (pH 7.4, 37°C). Optic nerve/chiasm preparations were treated with the same fixative for 1 hour at 4 °C and transferred to 30% sucrose overnight before embedding into OCT medium and snap freezing. For immunofluorescence labeling, sections were blocked in 10% normal donkey serum (NDS, Jackson ImmunoResearch, West Grove, PA) in PBS for 1 hour at room temperature prior to incubation with the following antibodies: guinea pig polyclonal anti-GFAP antibody (1:500; Advanced ImmunoChemical, Long Beach, CA), chick monoclonal anti-nestin antibody (1:100; Neuromics, Edina, MN), goat polyclonal anti-Brn3a antibody (1:1,000; Santa Cruz Biotechnology, Santa Cruz, CA), rabbit polyclonal anti-sox2 antibody (1:1,000;Chemicon, Temecular, CA), rabbit polyclonal anti-Iba1 antibody (1:100; Wako Pure Chemical Industries, Japan), rat monoclonal anti-CD31 antibody (1:500; BD Pharmingen, San Diego, CA), mouse monoclonal anti-neurofilament 68k antibody (1:500; Sigma, St. Louis, MO) and mouse monoclonal anti-S100β antibody (1:1,000, St. Louis, MO) in 10% NDS for 16 hours at 4°C. Fluorescence-conjugated secondary antibodies were applied at 1:100 dilution for 4 hours at 4 °C and then washed with PBS. For myelin staining, the sections were stained with FluoroMyelin (Invitrogen, Carlsbad, CA). All tissue sections were counterstained with the nucleic acid stain Hoechst 33342 (1 μg/ml; Invitrogen). Images were acquired with confocal microscopy (Olympus FluoView1000; Olympus, Tokyo, Japan). The numbers of activated microglia and new blood vessels were quantified by direct counting of representative matched areas (1024 × 1024 pixels per field) in the prechiasmal optic nerves and chiasm using a 60×1.4 NA microscope objective. Counting was performed on specimens from at least four mice of each group.

High Resolution Large Scale Mosaic Imaging, Electron Microscopy and Electron Microscope Tomography

Mice were deeply anesthetized with Nembutal (10 mg/100g body weight) and transcardially perfused with oxygenated Ringer's solution at 37°C, followed by 1.5% paraformaldehyde (PFA) and 2.5% glutaraldehyde in 0.1M sodium cacodylate buffer (pH 7.4). Optic nerve/chiasm were post-fixed in 1% OsO_4, post-stained with 2% uranyl acetate at 4°C, dehydrated through graded ethanol/acetone solutions, and embedded in Durcupan resin (Fluka, St. Louis, MO). For large scale mosaic imaging, semi-thin (0.5μm) sections were stained with toluidine-blue. Images were captured at 100X using an Olympus spinning disk confocal microscope (Olympus America Inc., Center Valley, PA) equipped with a motorized automated stage controlled by MicroBrightField Neurolucida software (MBF Bioscience Inc., Williston, VT).

For conventional EM, ultrathin (80-100 nm) sections were post-stained with uranyl acetate and lead salts prior to imaging using a JEOL JEM 1200EX transmission EM operated at 80kV. The negatives were digitized at 1800 dpi using a Nikon CoolScan system, giving an image size of 4033 × 6010 pixel array and a pixel resolution of 1.77 nm. For electron microscope tomography, semi-thick sections of optic nerve/chiasm from mice of each genotype were cut at a thickness of 400-500 nm. Sections were then stained for 30 minutes in 2% aqueous uranyl acetate, followed by 15 minutes in lead salts. Fiduciary cues consisting of 10 nm and 20 nm colloidal gold particles were deposited on opposite sides of the section. For each reconstruction, a series of images at regular tilt increments was collected with a JEOL JEM 4000EX intermediate voltage EM operated at 400 kV. The specimens were irradiated before initiating a tilt series to limit anisotropic specimen thinning during image collection. Tilt series were recorded on film at 6,000X magnification with an angular increment of 2° from −60° to +60° about an axis perpendicular to the optical axis of

the microscope using a computer-controlled goniometer to increment accurately the angular steps. The illumination was held to near parallel beam conditions and optical density maintained constant by varying the exposure time. The IMOD package (Mastronarde, 1997) was used for rough alignment with the fine alignment and reconstruction was performed using the TxBR package (NCMIR, UCSD, La Jolla, CA) (Lawrence et al., 2006). .

Retrograde Labeling of Retinal Ganglion Cells

One week prior to euthanasia, FluoroGold (1 μl/injection; Fluorochrome Inc., Englewood, CO) diluted in saline was microinjected bilaterally into the superior colliculi of anesthetized mice with a mixture of ketamine (Fort Dodge Animal Health) and xylazine (Vedeco Inc.) in a stereotactic apparatus, as previously described (Kim et al., 2004). Fluoro-Gold is taken up by the axon terminals of RGC neurons and transported retrogradely to the cell bodies in the retina (Selles-Navarro et al., 1996). The FluoroGold in the RGC neurons persists for at least 3 weeks without significant fading or leakage (Dong et al., 1996). Mosaic image arrays from retinal flat-mounts (n=6 retinal flat-mounts/mice/group) were captured under an Olympus spinning disk confocal microscope (Olympus America Inc., Center Valley, PA) equipped with a high-precision closed loop XY stage and closed loop Z control with commercial mosaic acquisition software from MicroBrightField (MBF Bioscience Inc., Williston, VT) modified by us (Chow et al., 2006, Price et al., 2006). The microscope was equipped with a high-resolution CCD camera for high-speed mosaic acquisition. Images were stored in Photoshop files (Adobe Systems Inc., San Jose, CA).

Statistical Analysis and Data Dissemination

The data are presented as the mean ± SD. Mice from each of the genotypes were evaluated using one-way analysis of variance (ANOVA) and the *t*-test with Bonferroni correction. High resolution large scale mosaic images described in this paper are available through the Cell Centered Database (http://ccdb.ucsd.edu) under project P2054.

RESULTS

Increased Neoplastic Astrocyte Proliferation in *Nf1*+/−^{GFAP}CKO Mouse Optic Glioma

Gross anatomical inspection of the optic chiasm/nerves from wild-type, *Nf1*+/−, and *Nf1*^{GFAP}CKO mice showed normal appearances at 9 months of age (Fig. 1A-C). In contrast, these regions in *Nf1*+/−^{GFAP}CKO mice appeared as gross fusiform enlargements involving the pre-chiasmatic optic nerves and optic chiasm (Fig. 1D). Previous studies on human glioma have demonstrated that the tumoral cells often express proteins typically found in neural stem or astroglial progenitor cells (sox2 and nestin) (Almqvist et al., 2002, Schmitz et al., 2007, Zhang et al., 2008, Gangemi et al., 2009, McCord et al., 2009). To determine whether the GFAP-immunoreactive cells in pre-chiasmatic optic nerves and chiasm of *Nf1*+/−^{GFAP}CKO mice were astrocytoma cells, we employed nestin and sox2 double labeling immunohistochemistry. As shown in Figure 1, GFAP-immunoreactive cells (astrocytes) with thin fibrillary processes were found in the pre-chiasmatic optic nerves and chiasm of wild-type, *Nf1*+/−, and *Nf1*^{GFAP}CKO mice (Fig. 1E-G, I-K, M-O and Q-S). In contrast, comparable regions of the optic pathway of *Nf1*+/−^{GFAP}CKO mice showed irregularly-shaped and thickened GFAP+ cells (astrocytes) (Fig. 1H, L, P and T). In addition, while nestin-immunoreactive cells were not observed in wild-type, *Nf1*+/−, or *Nf1*^{GFAP}CKO mouse optic nerves (Fig. 1I-K), *Nf1*+/−^{GFAP}CKO mouse had nestin-positive irregularly-shaped and thickened cells (Fig. 1L). Similarly, sox2-immunoreactive cells were rarely observed in wild-type, *Nf1*+/− and *Nf1*^{GFAP}CKO mice (Fig. 1M-O and Q-S), but were significantly increased in the optic nerves of *Nf1*+/−^{GFAP}CKO mice (Fig. 1P and T). Moreover, the GFAP+ or S100b+ glial cells in the optic pathway of these mice co-labeled with glioma-associated progenitor cell markers (sox2 and nestin; Fig. 1L and 1T),

supporting their classification as neoplastic astrocytes. Quantitative analysis revealed that the number of sox2+ cells was significantly increased in the pre-chiasmatic optic nerve and optic chiasm (Fig. 1U).

To evaluate ultrastructural changes in the pre-chiasmic optic nerves of *Nf1*+/−^{GFAP}CKO mice, we analyzed large samples at high resolution by recording wide-field mosaic images (~70 fields at 100X) of longitudinal sections of the optic chiasm/nerve stained with toluidine blue. Gross anatomical analysis of the optic chiasm/nerves from control mice showed a normal appearance at 9 months of age (Supplementary Fig. 1A-a), whereas optic gliomas appeared as gross thickenings and enlargements of the pre-chiasmic nerve in *Nf1*+/−^{GFAP}CKO mice (Supplementary Fig. 1B-b). Examination of electron micrographs revealed well-oriented bundles of axons near linearly-arranged columns of astrocytes within the pre-chiasmatic optic nerves of wild-type (not shown), *Nf1*+/− (not shown) and *Nf1*^{GFAP}CKO mice (Fig. 1V, Supplementary Fig. 1A). In striking contrast, we found hypercellular tumor cell nests, focal disruption of axon bundles, swelling and voids in individual axonal fibers, and associated lamellar spheroid arrays, as well as a lack of the linear orientation of fibers and glia observed in the *Nf1*^{GFAP}CKO mice (Fig. 1W, Supplementary Fig. 1B). Moreover, many cells within the tumor areas of *Nf1*+/−^{GFAP}CKO mouse optic nerves showed irregular nuclear morphology and an elongated cytoplasm, which contained many organelles and glial filaments (Supplementary Fig. 1D, F-H), suggesting that these cells are neoplastic astrocytes.

Nf1+/−^{GFAP}CKO Mouse Optic Gliomas Contain Microglia

Growing evidence indicates that microglia may play important roles in brain tumor formation and progression (Badie and Schartner, 2001, Graeber et al., 2002). Furthermore, recent studies from our group have shown that *Nf1*+/−microglia are critical cellular determinants of optic glioma growth and elaborate key growth factors and cytokines that increase the proliferation of *Nf1*-/- astrocytes (Daginakatte and Gutmann, 2007, Daginakatte et al., 2008). At 9 months of age, *Nf1*+/−^{GFAP}CKO mice have significantly more microglia than wild-type, *Nf1*+/− or *Nf1*^{GFAP}CKO mice (Fig. 2). These findings support the notion that optic glioma formation is associated with microglia infiltration.

Increased Vascularization in Nf1+/−^{GFAP}CKO Mouse Optic Glioma

To characterize new blood vessel formation in the gliomas of *Nf1*+/−^{GFAP}CKO mice, we performed CD31 immunohistochemistry, a marker for endothelial cells. As shown in Figure 3, we observed increased numbers of CD31-immunoreactive cells in the pre-chiasmatic optic nerves of *Nf1*+/−^{GFAP}CKO mice (Fig. 3D) compared to wild-type, *Nf1*+/− and *Nf1*^{GFAP}CKO mice (Fig. 3A-C). Quantitation revealed that the number of CD31+ cells was significantly increased in the pre-chiasmatic optic nerve and optic chiasm (Fig. 3E).

Abnormal Optic Nerve Axon Organization in *Nf1*+/−^{GFAP}CKO Mice

To determine whether optic glioma formation results in changes in axonal organization, we performed double-labeling immunohistochemistry for both GFAP (astrocytes) and neurofilament 68k (axons). As shown in Figure 4, astrocytes with elongated processes and well-oriented axonal fiber projections were present in the pre-chiasmatic optic nerves of wild-type, *Nf1*+/−, and *Nf1*^{GFAP}CKO mice (Fig. 4A-C, E-G and M-O). In contrast, comparable regions from *Nf1*+/−^{GFAP}CKO mice showed irregularly shaped and thickened astrocytes (Fig. 4D, H and P) and disoriented axonal fiber projections associated with axonal swelling (Fig. 4D, L and P). These findings indicate that glioma formation results in disorganization of the normal optic nerve axonal architecture.

Axonal and Myelin Degeneration in the *Nf1*+/−^{GFAP}CKO Mouse Optic Nerve

To determine whether optic glioma formation induces axonal and myelin degeneration, we performed FluoroMyelin staining and transmission EM or EM tomography. FluoroMyelin staining (Fig. 5A) and EM analysis (Fig. 5Aa) showed a large number of healthy-looking cross-sectional axonal profiles of pre-chiasmatic optic nerves in *Nf1*^{GFAP}CKO mice. In contrast, comparable regions from *Nf1*+/−^{GFAP}CKO mice showed the presence of severe alterations, including disruption of myelin, hypermyelination, spherical lamellar bodies and focal disruption of axon bundles (Fig. 5B, 5Bb).

Using EM tomography, 3D reconstruction images revealed the linear orientation of axonal fibers in *Nf1*^{GFAP}CKO mouse optic nerves (Fig. 5C, 5E). In contrast, comparable regions of the optic nerves from *Nf1*+/−^{GFAP}CKO mice showed marked disorientation of axonal fiber projections and myelin degeneration (Fig. 5D, 5F). Interestingly, many axons with internodal lamellar spheroid bodies were associated with axons exhibiting various stages of degeneration. Chronic abnormalities of myelination were evidenced by hypermyelination surrounding multiple fibers (Fig. 5D). Moreover, compared with *Nf1*^{GFAP}CKO mice (Fig. 5G), the pre-chiasmatic optic nerves from *Nf1*+/−^{GFAP}CKO mice exhibited nodal blebs with loss of subaxolemmal density and disorganized paranodes (Fig. 5H) as well as accumulation of dense bodies within the swollen axons (Fig. 5I). No differences in optic nerve ultrastructure were observed in 9 month-old wild-type or *Nf1*+/− mice (data not shown).

RGC loss in *Nf1*+/−^{GFAP}CKO Mice

To assess RGC loss in *Nf1*+/−^{GFAP}CKO mice with optic glioma, we retrogradely labeled RGC neurons by FluoroGold injection into the superior colliculus. Mean RGC densities per retina for each group are presented in Table 1. As shown in Figure 7, *Nf1*+/−^{GFAP}CKO mice exhibited significantly reduced numbers of RGC neurons (32.9% in the central, 31.3% in the middle, and 41.9% in the peripheral areas) compared to wild-type (Fig. 6A, B and Fig. 7), *Nf1*+/− (Fig. 6C, D and Fig. 7) and *Nf1*^{GFAP}CKO mice (Fig. 6E, F and Fig. 7). In addition, RGC loss was significant in the peripheral areas of *Nf1*+/− and *Nf1*^{GFAP}CKO mice (Fig. 7). To provide additional confirmatory evidence for RGC loss, we also labeled whole mount retinas with Brn3a, an antibody specific for RGCs (Nadal-Nicolas et al., 2009,Raymond et al., 2009). Brn3a labeling of *Nf1*+/−^{GFAP}CKO mice showed a similar pattern of RGC loss compared to FluoroGold labeling (Supplementary Fig. 2).

DISCUSSION

Previous studies from our group have shown that optic glioma formation in *Nf1*+/−^{GFAP}CKO mice begins with increased astrocyte proliferation coupled with increased numbers of microglia and endothelial cells in the evolving tumor surround at 6 weeks of age (Bajenaru et al., 2003, Bajenaru et al., 2005). Optic gliomas are readily detected by magnetic resonance imaging (MRI) and gross inspection in 95-98% of these mice by 3 months of age (Bajenaru et al., 2003, Bajenaru et al., 2005, Banerjee et al., 2007). In addition, there is accompanying axonal disorganization in the optic nerve as well as RGC apoptosis at the time of glioma detection (Hegedus et al., 2009). Collectively, these observations suggest a temporal course of tumor evolution in which increased astrocyte (glial cell) proliferation and associated stromal changes advance over a period of 6 weeks to radiologically-evident neoplasia and neuronal dysfunction.

While these reports provide important information about early tumor evolution, they raise important questions about events subsequent to glioma formation. First, do the GFAP+ cells in the tumors represent reactive glial cells as suggested by Parada and colleagues (Zhu et al., 2005) or true neoplastic glia? Second, what is the relationship between stromal cells and

neoplastic glia beyond 3 months of age? Third, is optic nerve degeneration a progressive process in *Nf1*+/−^{GFAP}CKO mice?

The distinction between hyperproliferating, reactive astrocytes (gliosis) and neoplasia has not been firmly established in genetically-engineered mouse models of cancer. Morphologically, reactive astrocytes have thickened processes and intense GFAP immunoreactivity, similar to neoplastic glial cells. These morphological changes were detected in some of the cells in the *Nf1*+/−^{GFAP}CKO mouse optic glioma specimens (Bajenaru et al., 2003); however, we observed additional features in optic glioma astrocytes that support the classification of these lesions as tumors. Using electron microscopy, astrocytes with prominent glial filaments also exhibited irregular, elongated nuclei (nuclear atypia) and small membrane bound organelles, including mitochondria. This is consistent with prior studies demonstrating that astrocytoma tumor cells are elongated ("piloid") and contain many glial filaments as well as contain cytoplasm rich in organelles and mitochondria (Scheithauer and Bruner, 1987, Liberski and Kordek, 1997, Liberski, 1998).

In addition to cellular morphology, lineage markers are frequently employed to distinguish differentiated astrocytes from neoplastic astrocytes. Two commonly used markers are nestin and sox2, which are typically expressed by progenitor cells. As have been described in human gliomas, *Nf1*+/−^{GFAP}CKO mouse optic glioma cells expressing GFAP or S100b also co-expressed nestin or sox2. It should be were also immunoreactive for nestin or sox2, supporting the existence of a limited progenitor cell population within these tumors. These results are consistent with previous studies demonstrating that small clusters of immature progenitors expand to populate the tumor (Hemmati et al., 2003, Singh et al., 2003). It is not known whether optic glioma formation is associated with the de-differentiation of neoplastic astrocytes to a less mature, progenitor-like cell, or whether tumors arise following *Nf1* inactivation in progenitor cells present in the pediatric optic nerve, as has been debated for high-grade gliomas (Bachoo et al., 2002, Uhrbom et al., 2002, Dai and Holland, 2003). Additional studies are in progress to address the cell of origin of optic glioma.

Recent studies from our group and others have demonstrated that the tumor microenvironment is critical for nervous system tumor development in the context of the NF1 inherited cancer syndrome. Both central nervous system (CNS) gliomas (Bajenaru et al., 2003, Zhu et al., 2005) and peripheral nervous system (PNS) neurofibromas (Zhu et al., 2002, Yang et al., 2008, Le et al., 2009) require *Nf1* stromal heterozygosity coupled with *Nf1* loss in preneoplastic cells (e.g., Schwann and glial cell precursors). Bi-allelic loss of *NF1* gene expression in NF1-associated patient neurofibromas (Colman et al., 1995, Perry et al., 2001) and gliomas (Gutmann et al., 2000, Kluwe et al., 2001) has previously been demonstrated, and in combination with *NF1*+/− stromal cell types, culminates in benign nervous system tumor formation. In the PNS, mast cells produce soluble factors that drive neurofibroma formation (Yang et al., 2006), while brain microglia elaborate paracrine growth and survival molecules that facilitate glioma formation in the CNS (Daginakatte and Gutmann, 2007, Warrington et al., 2007). In the current study, we report increased numbers of microglia in the vicinity of the optic glioma. This increase in microglia does not reflect *Nf1* heterozygosity alone or a response to *Nf1* glial cell loss, but is most likely a consequence of glioma formation. In addition, we observed more vascularity in response to tumor formation, as evidenced by increased numbers of CD31+ endothelial cells. This is consistent with our previous study (Bajenaru et al., 2005) and extends these findings to a much later time point in glioma development. In human low-grade glioma tumors, ultrathin section microscopy studies have demonstrated endothelial hyperplasia, surface in-folding of endothelial cells, and irregularities of the basal lamina (Shibata, 1989, Takeuchi et al., 2004), similar to what we observed in the mouse optic gliomas. Moreover, the finding of increased vascularity in the murine optic glioma tumors parallels the increased contrast

enhancement on MRI observed in human NF1-associated optic glioma (Perilongo et al., 1999, Jost et al., 2008). Future studies will be required to determine whether microglial infiltration precedes endothelial proliferation during optic glioma evolution.

Finally, we sought to determine whether axonal degeneration and RGC neuronal loss is a progressive process in *Nf1*+/−^{GFAP}CKO mouse optic gliomas. Previously, we showed that RGC neuronal death is not observed at 6 weeks of age, but is easily detected by 3 months of age (Hegedus et al., 2009). Whereas wild-type, *Nf1*+/−, and *Nf1*^{GFAP}CKO mice at 3 months of age have fewer than 5% TUNEL+ RGC neurons, *Nf1*+/−^{GFAP}CKO mice exhibit 15-20% TUNEL+ RGC neurons. While the percentage of TUNEL+ (apoptotic) RGC neurons was not directly measured in *Nf1*+/−^{GFAP}CKO mice at 9 months of age, we observed a 36% reduction in the total number of RGC neurons. As before, *Nf1*+/−, and *Nf1*^{GFAP}CKO mice at 9 months of age have similar numbers of RGC neurons. Based on the findings in this study and our previous report (Hegedus et al., 2009), we hypothesize that RGC neuron loss results from early changes in axonal integrity as a direct consequence of glioma development. Studies are currently underway to define the temporal course of RGC death from optic glioma. It should be noted that the neuronal loss is a consequence of *Nf1* optic glioma formation, not *Nf1* loss in RGCs. Using Rosa-YFP reporter mice, we previously reported that the Cre activity in the GFAP-Cre transgenic mouse line used to drive *Nf1* loss leads to recombination in some retinal astrocytes, but not in retinal neurons (Hegedus et al., 2009) or oligodendrocytes (Hegedus, unpublished observations). These findings support our finding that most of the astrocytes in the mouse optic nerve are deficient for *Nf1* gene expression, while the neurons and microglia have reduced *Nf1* expression (*Nf1*+/− cells).

Axonal injury is known to cause changes in RGC neuronal function, eventually resulting in death (Quigley et al., 1995, Morgan, 2000, Wax and Tezel, 2002, Osborne et al., 2004, Buckingham et al., 2008). In light of our finding of axonal degeneration, it is likely that loss of axonal integrity perturbs rapid anterograde and retrograde axonal transport in the optic nerve, as has reported for other optic nerve pathologic states (Anderson and Hendrickson, 1974, Minckler et al., 1977, Johnson et al., 2000, Pease et al., 2000, Quigley et al., 2000, Levin and Gordon, 2002). Present experiments are aimed at identifying the signaling pathways deranged in *Nf1*+/− RGC neurons that predispose these cells to axonal degeneration and apoptosis in the context of glioma formation. In this regard, recent studies from our laboratory have shown that *Nf1*+/− RGC neurons have reduced neurite lengths, growth cone diameters, and survival, which reflect reduced cyclic AMP levels *in vitro* and *in vivo* (Brown JA et al., J. Neurosci 2010).

In summary, our findings demonstrate that the combination of optic nerve *Nf1* heterozygosity and glial cell *Nf1* loss results in disrupted axonal-glial relationships, which culminate in the degeneration of optic nerve axons and, ultimately, the loss of their parent RGC neurons. The ability to define the responsible stromal cell types and developmental windows of RGC neuronal susceptibility in this preclinical mouse model of NF1-associated optic glioma affords unique opportunities to develop treatment strategies that target the correct cells in the tumor microenvironment at the correct time during tumor evolution and growth to optimally reduce glioma-associated damage.

Supplementary Material

Refer to Web version on PubMed Central for supplementary material.

Acknowledgments

This research was supported by grants from the National Cancer Institute (NCI U01-CA141549-01) and National Center for Research Resources (P41 RR004050). The Cell Centered Database is supported by NIH grants from

NCRR RR004050, RR RR08605 and the Human Brain Project DA016602 from the National Institute on Drug Abuse, the National Institute of Biomedical Imaging and Bioengineering and the National Institute of Mental Health. We thank Masako Terada, Hiroyuki Hakozaki and Ohkyung Kwon for their excellent technical assistance, and Eric Bushong for critical reading of manuscript.

Supporting grants: NCI UO1-CA84314 (to DHG and MHE) and NCRR P41 RR004050 (MHE)

REFERENCES

Almqvist PM, Mah R, Lendahl U, Jacobsson B, Hendson G. Immunohistochemical detection of nestin in pediatric brain tumors. J Histochem Cytochem. 2002; 50:147–158. [PubMed: 11799134]

Anderson DR, Hendrickson A. Effect of intraocular pressure on rapid axoplasmic transport in monkey optic nerve. Invest Ophthalmol. 1974; 13:771–783. [PubMed: 4137635]

Bachoo RM, Maher EA, Ligon KL, Sharpless NE, Chan SS, You MJ, Tang Y, DeFrances J, Stover E, Weissleder R, Rowitch DH, Louis DN, DePinho RA. Epidermal growth factor receptor and Ink4a/Arf: convergent mechanisms governing terminal differentiation and transformation along the neural stem cell to astrocyte axis. Cancer Cell. 2002; 1:269–277. [PubMed: 12086863]

Badie B, Schartner J. Role of microglia in glioma biology. Microsc Res Tech. 2001; 54:106–113. [PubMed: 11455617]

Bajenaru ML, Garbow JR, Perry A, Hernandez MR, Gutmann DH. Natural history of neurofibromatosis 1-associated optic nerve glioma in mice. Ann Neurol. 2005; 57:119–127. [PubMed: 15622533]

Bajenaru ML, Hernandez MR, Perry A, Zhu Y, Parada LF, Garbow JR, Gutmann DH. Optic nerve glioma in mice requires astrocyte Nf1 gene inactivation and Nf1 brain heterozygosity. Cancer Res. 2003; 63:8573–8577. [PubMed: 14695164]

Bajenaru ML, Zhu Y, Hedrick NM, Donahoe J, Parada LF, Gutmann DH. Astrocyte-specific inactivation of the neurofibromatosis 1 gene (NF1) is insufficient for astrocytoma formation. Mol Cell Biol. 2002; 22:5100–5113. [PubMed: 12077339]

Balcer LJ, Liu GT, Heller G, Bilaniuk L, Volpe NJ, Galetta SL, Molloy PT, Phillips PC, Janss AJ, Vaughn S, Maguire MG. Visual loss in children with neurofibromatosis type 1 and optic pathway gliomas: relation to tumor location by magnetic resonance imaging. Am J Ophthalmol. 2001; 131:442–445. [PubMed: 11292406]

Banerjee D, Hegedus B, Gutmann DH, Garbow JR. Detection and measurement of neurofibromatosis-1 mouse optic glioma in vivo. Neuroimage. 2007; 35:1434–1437. [PubMed: 17383899]

Buckingham BP, Inman DM, Lambert W, Oglesby E, Calkins DJ, Steele MR, Vetter ML, Marsh-Armstrong N, Horner PJ. Progressive ganglion cell degeneration precedes neuronal loss in a mouse model of glaucoma. J Neurosci. 2008; 28:2735–2744. [PubMed: 18337403]

Chow SK, Hakozaki H, Price DL, MacLean NA, Deerinck TJ, Bouwer JC, Martone ME, Peltier ST, Ellisman MH. Automated microscopy system for mosaic acquisition and processing. J Microsc. 2006; 222:76–84. [PubMed: 16774516]

Colman SD, Williams CA, Wallace MR. Benign neurofibromas in type 1 neurofibromatosis (NF1) show somatic deletions of the NF1 gene. Nat Genet. 1995; 11:90–92. [PubMed: 7550323]

Daginakatte GC, Gianino SM, Zhao NW, Parsadanian AS, Gutmann DH. Increased c-Jun-NH2-kinase signaling in neurofibromatosis-1 heterozygous microglia drives microglia activation and promotes optic glioma proliferation. Cancer Res. 2008; 68:10358–10366. [PubMed: 19074905]

Daginakatte GC, Gutmann DH. Neurofibromatosis-1 (Nf1) heterozygous brain microglia elaborate paracrine factors that promote Nf1-deficient astrocyte and glioma growth. Hum Mol Genet. 2007; 16:1098–1112. [PubMed: 17400655]

Dai C, Holland EC. Astrocyte differentiation states and glioma formation. Cancer J. 2003; 9:72–81. [PubMed: 12784872]

Dalla Via P, Opocher E, Pinello ML, Calderone M, Viscardi E, Clementi M, Battistella PA, Laverda AM, Da Dalt L, Perilongo G. Visual outcome of a cohort of children with neurofibromatosis type 1 and optic pathway glioma followed by a pediatric neurooncology program. Neuro Oncol. 2007; 9:430–437. [PubMed: 17704361]

Dong K, Ahmed AK, Qu T, Sugioka K, Yamada K, Yamadori T. Retrograde fluorescent double-labeling study of bilaterally projecting retinal ganglion cells in albino rats at different stages of development. Brain Res Dev Brain Res. 1996; 95:55–62.

Friedman JM. Epidemiology of neurofibromatosis type 1. Am J Med Genet. 1999; 89:1–6. [PubMed: 10469430]

Gangemi RM, Griffero F, Marubbi D, Perera M, Capra MC, Malatesta P, Ravetti GL, Zona GL, Daga A, Corte G. SOX2 silencing in glioblastoma tumor-initiating cells causes stop of proliferation and loss of tumorigenicity. Stem Cells. 2009; 27:40–48. [PubMed: 18948646]

Graeber MB, Scheithauer BW, Kreutzberg GW. Microglia in brain tumors. Glia. 2002; 40:252–259. [PubMed: 12379912]

Gutmann DH, Donahoe J, Brown T, James CD, Perry A. Loss of neurofibromatosis 1 (NF1) gene expression in NF1-associated pilocytic astrocytomas. Neuropathol Appl Neurobiol. 2000; 26:361–367. [PubMed: 10931370]

Hegedus B, Banerjee D, Yeh TH, Rothermich S, Perry A, Rubin JB, Garbow JR, Gutmann DH. Preclinical cancer therapy in a mouse model of neurofibromatosis-1 optic glioma. Cancer Res. 2008; 68:1520–1528. [PubMed: 18316617]

Hegedus B, Hughes FW, Garbow JR, Gianino S, Banerjee D, Kim K, Ellisman MH, Brantley MA Jr. Gutmann DH. Optic nerve dysfunction in a mouse model of neurofibromatosis-1 optic glioma. J Neuropathol Exp Neurol. 2009; 68:542–551. [PubMed: 19525901]

Hemmati HD, Nakano I, Lazareff JA, Masterman-Smith M, Geschwind DH, Bronner-Fraser M, Kornblum HI. Cancerous stem cells can arise from pediatric brain tumors. Proc Natl Acad Sci U S A. 2003; 100:15178–15183. [PubMed: 14645703]

Johnson EC, Deppmeier LM, Wentzien SK, Hsu I, Morrison JC. Chronology of optic nerve head and retinal responses to elevated intraocular pressure. Invest Ophthalmol Vis Sci. 2000; 41:431–442. [PubMed: 10670473]

Jost SC, Ackerman JW, Garbow JR, Manwaring LP, Gutmann DH, McKinstry RC. Diffusion-weighted and dynamic contrast-enhanced imaging as markers of clinical behavior in children with optic pathway glioma. Pediatr Radiol. 2008; 38:1293–1299. [PubMed: 18846370]

Kim KY, Ju WK, Neufeld AH. Neuronal susceptibility to damage: comparison of the retinas of young, old and old/caloric restricted rats before and after transient ischemia. Neurobiol Aging. 2004; 25:491–500. [PubMed: 15013570]

Kluwe L, Hagel C, Tatagiba M, Thomas S, Stavrou D, Ostertag H, von Deimling A, Mautner VF. Loss of NF1 alleles distinguish sporadic from NF1-associated pilocytic astrocytomas. J Neuropathol Exp Neurol. 2001; 60:917–920. [PubMed: 11556548]

Lawrence A, Bouwer JC, Perkins G, Ellisman MH. Transform-based backprojection for volume reconstruction of large format electron microscope tilt series. J Struct Biol. 2006; 154:144–167. [PubMed: 16542854]

Le LQ, Shipman T, Burns DK, Parada LF. Cell of origin and microenvironment contribution for NF1-associated dermal neurofibromas. Cell Stem Cell. 2009; 4:453–463. [PubMed: 19427294]

Levin LA, Gordon LK. Retinal ganglion cell disorders: types and treatments. Prog Retin Eye Res. 2002; 21:465–484. [PubMed: 12207946]

Liberski PP. The ultrastructure of glial tumors of astrocytic lineage: a review. Folia Neuropathol. 1998; 36:161–177. [PubMed: 9833393]

Liberski PP, Kordek R. Ultrastructural pathology of glial brain tumors revisited: a review. Ultrastruct Pathol. 1997; 21:1–31. [PubMed: 9029763]

Listernick R, Charrow J, Greenwald M, Mets M. Natural history of optic pathway tumors in children with neurofibromatosis type 1: a longitudinal study. J Pediatr. 1994; 125:63–66. [PubMed: 8021787]

Listernick R, Charrow J, Greenwald MJ, Esterly NB. Optic gliomas in children with neurofibromatosis type 1. J Pediatr. 1989; 114:788–792. [PubMed: 2497236]

Listernick R, Darling C, Greenwald M, Strauss L, Charrow J. Optic pathway tumors in children: the effect of neurofibromatosis type 1 on clinical manifestations and natural history. J Pediatr. 1995; 127:718–722. [PubMed: 7472822]

Listernick R, Ferner RE, Piersall L, Sharif S, Gutmann DH, Charrow J. Late-onset optic pathway tumors in children with neurofibromatosis 1. Neurology. 2004; 63:1944–1946. [PubMed: 15557519]

Listernick R, Louis DN, Packer RJ, Gutmann DH. Optic pathway gliomas in children with neurofibromatosis 1: consensus statement from the NF1 Optic Pathway Glioma Task Force. Ann Neurol. 1997; 41:143–149. [PubMed: 9029062]

Mastronarde DN. Dual-axis tomography: an approach with alignment methods that preserve resolution. J Struct Biol. 1997; 120:343–352. [PubMed: 9441937]

McCord AM, Jamal M, Shankavarum UT, Lang FF, Camphausen K, Tofilon PJ. Physiologic oxygen concentration enhances the stem-like properties of CD133+ human glioblastoma cells in vitro. Mol Cancer Res. 2009; 7:489–497. [PubMed: 19372578]

Minckler DS, Bunt AH, Johanson GW. Orthograde and retrograde axoplasmic transport during acute ocular hypertension in the monkey. Invest Ophthalmol Vis Sci. 1977; 16:426–441. [PubMed: 67096]

Morgan JE. Optic nerve head structure in glaucoma: astrocytes as mediators of axonal damage. Eye. 2000; 14(Pt 3B):437–444. [PubMed: 11026971]

Nadal-Nicolas FM, Jimenez-Lopez M, Sobrado-Calvo P, Nieto-Lopez L, Canovas-Martinez I, Salinas-Navarro M, Vidal-Sanz M, Agudo M. Brn3a as a marker of retinal ganglion cells: qualitative and quantitative time course studies in naive and optic nerve-injured retinas. Invest Ophthalmol Vis Sci. 2009; 50:3860–3868. [PubMed: 19264888]

Osborne NN, Chidlow G, Layton CJ, Wood JP, Casson RJ, Melena J. Optic nerve and neuroprotection strategies. Eye. 2004; 18:1075–1084. [PubMed: 15534592]

Pease ME, McKinnon SJ, Quigley HA, Kerrigan-Baumrind LA, Zack DJ. Obstructed axonal transport of BDNF and its receptor TrkB in experimental glaucoma. Invest Ophthalmol Vis Sci. 2000; 41:764–774. [PubMed: 10711692]

Perilongo G, Moras P, Carollo C, Battistella A, Clementi M, Laverda A, Murgia A. Spontaneous partial regression of low-grade glioma in children with neurofibromatosis-1: a real possibility. J Child Neurol. 1999; 14:352–356. [PubMed: 10385841]

Perry A, Roth KA, Banerjee R, Fuller CE, Gutmann DH. NF1 deletions in S-100 protein-positive and negative cells of sporadic and neurofibromatosis 1 (NF1)-associated plexiform neurofibromas and malignant peripheral nerve sheath tumors. Am J Pathol. 2001; 159:57–61. [PubMed: 11438454]

Price DL, Chow SK, Maclean NA, Hakozaki H, Peltier S, Martone ME, Ellisman MH. High-resolution large-scale mosaic imaging using multiphoton microscopy to characterize transgenic mouse models of human neurological disorders. Neuroinformatics. 2006; 4:65–80. [PubMed: 16595859]

Quigley HA, Guy J, Anderson DR. Blockade of rapid axonal transport. Effect of intraocular pressure elevation in primate optic nerve. Arch Ophthalmol. 1979; 97:525–531. [PubMed: 84662]

Quigley HA, McKinnon SJ, Zack DJ, Pease ME, Kerrigan-Baumrind LA, Kerrigan DF, Mitchell RS. Retrograde axonal transport of BDNF in retinal ganglion cells is blocked by acute IOP elevation in rats. Invest Ophthalmol Vis Sci. 2000; 41:3460–3466. [PubMed: 11006239]

Quigley HA, Nickells RW, Kerrigan LA, Pease ME, Thibault DJ, Zack DJ. Retinal ganglion cell death in experimental glaucoma and after axotomy occurs by apoptosis. Invest Ophthalmol Vis Sci. 1995; 36:774–786. [PubMed: 7706025]

Raymond ID, Pool AL, Vila A, Brecha NC. A Thy1-CFP DBA/2J mouse line with cyan fluorescent protein expression in retinal ganglion cells. Vis Neurosci. 2009; 26:453–465. [PubMed: 19930759]

Scheithauer BW, Bruner JM. The ultrastructural spectrum of astrocytic neoplasms. Ultrastruct Pathol. 1987; 11:535–581. [PubMed: 3318059]

Schmitz M, Temme A, Senner V, Ebner R, Schwind S, Stevanovic S, Wehner R, Schackert G, Schackert HK, Fussel M, Bachmann M, Rieber EP, Weigle B. Identification of SOX2 as a novel glioma-associated antigen and potential target for T cell-based immunotherapy. Br J Cancer. 2007; 96:1293–1301. [PubMed: 17375044]

Selles-Navarro I, Villegas-Perez MP, Salvador-Silva M, Ruiz-Gomez JM, Vidal-Sanz M. Retinal ganglion cell death after different transient periods of pressure-induced ischemia and survival intervals. A quantitative in vivo study. Invest Ophthalmol Vis Sci. 1996; 37:2002–2014. [PubMed: 8814140]

Shibata S. Ultrastructure of capillary walls in human brain tumors. Acta Neuropathol. 1989; 78:561–571. [PubMed: 2554636]

Singh SK, Clarke ID, Terasaki M, Bonn VE, Hawkins C, Squire J, Dirks PB. Identification of a cancer stem cell in human brain tumors. Cancer Res. 2003; 63:5821–5828. [PubMed: 14522905]

Takeuchi H, Kubota T, Sato K, Arishima H. Ultrastructure of capillary endothelium in pilocytic astrocytomas. Brain Tumor Pathol. 2004; 21:23–26. [PubMed: 15696965]

Thiagalingam S, Flaherty M, Billson F, North K. Neurofibromatosis type 1 and optic pathway gliomas: follow-up of 54 patients. Ophthalmology. 2004; 111:568–577. [PubMed: 15019338]

Uhrbom L, Dai C, Celestino JC, Rosenblum MK, Fuller GN, Holland EC. Ink4a-Arf loss cooperates with KRas activation in astrocytes and neural progenitors to generate glioblastomas of various morphologies depending on activated Akt. Cancer Res. 2002; 62:5551–5558. [PubMed: 12359767]

Warrington NM, Woerner BM, Daginakatte GC, Dasgupta B, Perry A, Gutmann DH, Rubin JB. Spatiotemporal differences in CXCL12 expression and cyclic AMP underlie the unique pattern of optic glioma growth in neurofibromatosis type 1. Cancer Res. 2007; 67:8588–8595. [PubMed: 17875698]

Wax MB, Tezel G. Neurobiology of glaucomatous optic neuropathy: diverse cellular events in neurodegeneration and neuroprotection. Mol Neurobiol. 2002; 26:45–55. [PubMed: 12392055]

Wolsey DH, Larson SA, Creel D, Hoffman R. Can screening for optic nerve gliomas in patients with neurofibromatosis type I be performed with visual-evoked potential testing? J AAPOS. 2006; 10:307–311. [PubMed: 16935228]

Yang FC, Chen S, Clegg T, Li X, Morgan T, Estwick SA, Yuan J, Khalaf W, Burgin S, Travers J, Parada LF, Ingram DA, Clapp DW. Nf1+/− mast cells induce neurofibroma like phenotypes through secreted TGF-beta signaling. Hum Mol Genet. 2006; 15:2421–2437. [PubMed: 16835260]

Yang FC, Ingram DA, Chen S, Zhu Y, Yuan J, Li X, Yang X, Knowles S, Horn W, Li Y, Zhang S, Yang Y, Vakili ST, Yu M, Burns D, Robertson K, Hutchins G, Parada LF, Clapp DW. Nf1-dependent tumors require a microenvironment containing Nf1+/−- and c-kit-dependent bone marrow. Cell. 2008; 135:437–448. [PubMed: 18984156]

Zhang M, Song T, Yang L, Chen R, Wu L, Yang Z, Fang J. Nestin and CD133: valuable stem cell-specific markers for determining clinical outcome of glioma patients. J Exp Clin Cancer Res. 2008; 27:85. [PubMed: 19108713]

Zhu Y, Ghosh P, Charnay P, Burns DK, Parada LF. Neurofibromas in NF1: Schwann cell origin and role of tumor environment. Science. 2002; 296:920–922. [PubMed: 11988578]

Zhu Y, Harada T, Liu L, Lush ME, Guignard F, Harada C, Burns DK, Bajenaru ML, Gutmann DH, Parada LF. Inactivation of NF1 in CNS causes increased glial progenitor proliferation and optic glioma formation. Development. 2005; 132:5577–5588. [PubMed: 16314489]

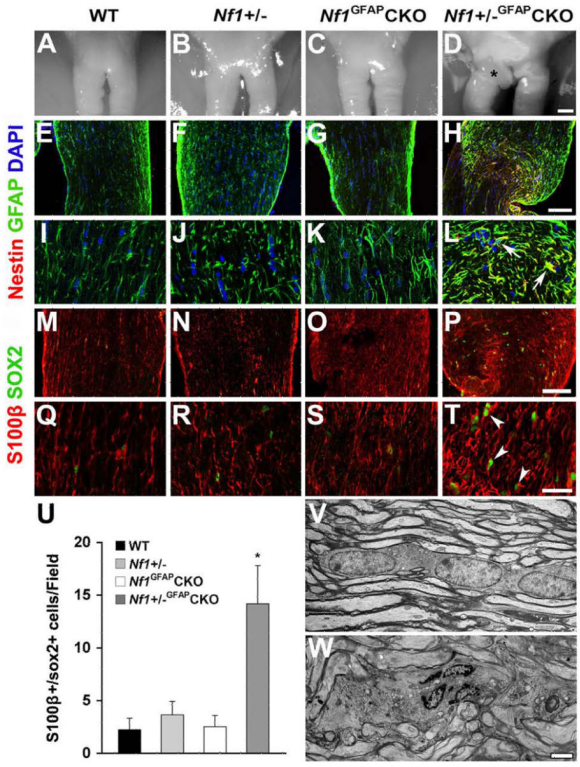

Fig. 1.

Neoplastic astrocytes in the pre-chiasmatic optic nerves of *Nf1*+/−^{GFAP}CKO mice. Sections from 9-month-old wild-type (A, E, I, M, Q, U), *Nf1*+/− (B, F, J, N, R, U), *Nf1*^{GFAP}CKO (C, G, K, O, S, U, V) and *Nf1*+/−^{GFAP}CKO (D, H, L, P, T, U, W) mice. Gross appearance of representative optic chiasm/nerves from these mice. No pathological changes were observed in wild-type (A), *Nf1*+/− (B) or *Nf1*^{GFAP}CKO mice (C), whereas *Nf1*+/−^{GFAP}CKO mouse optic nerves showed gross thickening and focal enlargement in the pre-chiasmatic optic nerve and chiasm (D; Asterisk). No nestin-positive astrocytes with elongated processes were observed in the prechiasmatic optic nerves and chiasm of wild-type (E, I), *Nf1*+/− (F, J) and *Nf1*^{GFAP}CKO mice (G, K), In contrast, the pre-chiasmatic optic nerves and chiasm of *Nf1*+/−^{GFAP}CKO mice have irregularly-shaped and thickened nestin- and GFAP-double positive cells (H, L, Arrows.). Rare sox2-positive cells with elongated processes were found in the pre-chiasmatic optic nerves and chiasm of wild-type (M, Q), *Nf1*+/− (N, R) and *Nf1*^{GFAP}CKO mice (O, S). In contrast, the pre-chiasmatic optic nerves and chiasm from *Nf1*+/−^{GFAP}CKO mice had increased numbers of sox2- and S100b-double positive cells (P, T, Arrowheads). Quantitation of sox2+ cells is shown in panel U. Error bar=SD. * $P < 0.05$ compared to wild-type mice, $n = 5$ optic nerve sections/mouse/group. The axons and glial cells in the pre-chiasmatic optic nerves and chiasm of *Nf1*^{GFAP}CKO mouse were indistinguishable from wild-type mice (Fig. 1V). In contrast, comparable regions from *Nf1*+/−^{GFAP}CKO mice showed hypercellular tumor cell nests and focal disruption of optic nerve fiber tracts (Fig. 1W). Scale bars: (A-D) 100 μm; (E-H, M-P) 50 μm; (I-L, Q-T) 20 μm; (V, W) 2 μm.

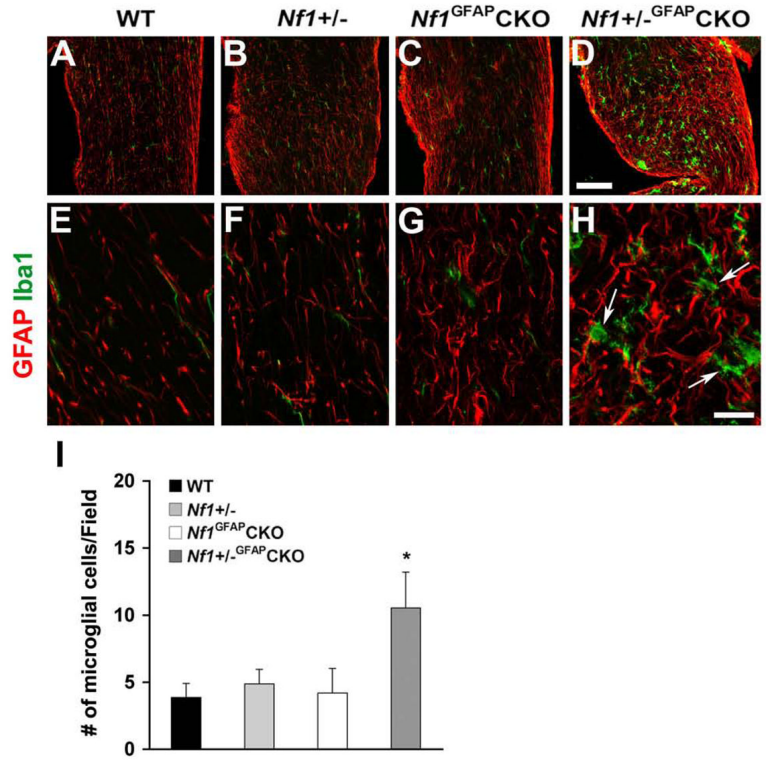

Fig. 2.

Increased microglia in the pre-chiasmatic optic nerves of *Nf1*+/−^{GFAP}CKO mice. Sections from 9-month-old wild-type (A, E), *Nf1*+/− (B, F), *Nf1*^{GFAP}CKO (C, G) and *Nf1*+/−^{GFAP}CKO (D, H) mice were immunostained with Iba1 and GFAP antibodies. Ramified, quiescent microglia were observed in wild-type (A, E), *Nf1*+/− (B, F) and *Nf1*^{GFAP}CKO mice (C, G). In contrast, increased numbers of microglia with thickened processes were found in the pre-chiasmatic optic nerves from *Nf1*+/−^{GFAP}CKO mice (D, H). Quantitation is shown in panel I. Error bar=SD. * $P < 0.05$ compared to wild-type mice, $n = 5$ optic nerve sections/mouse/group. Scale bars: (A-D) 50 μm; (E-H) 10 μm.

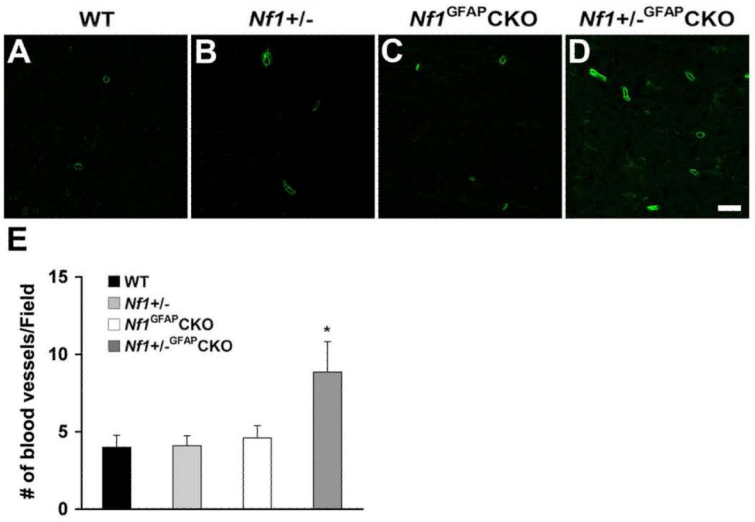

Fig. 3.

Increased numbers of endothelial cells in the pre-chiasmatic optic nerves of *Nf1*+/−GFAPCKO mice. Sections from 9-month-old wild-type (A), *Nf1*+/− (B), *Nf1*GFAPCKO (C) and *Nf1*+/−GFAPCKO (D) mice were stained with CD31 antibodies. Few scattered small blood vessels were observed in wild-type (A), *Nf1*+/− (B) and *Nf1*GFAPCKO (C) mouse optic nerves. In contrast, increased numbers of CD31+ cells were found in the pre-chiasmatic optic nerves of *Nf1*+/−GFAPCKO mice (D, H). Quantitation is shown in panel E. Error bar=SD. * $P < 0.05$ compared to wild-type mice, $n = 5$ optic nerve sections/mouse/group. Scale bars: (A-D) 10 μm.

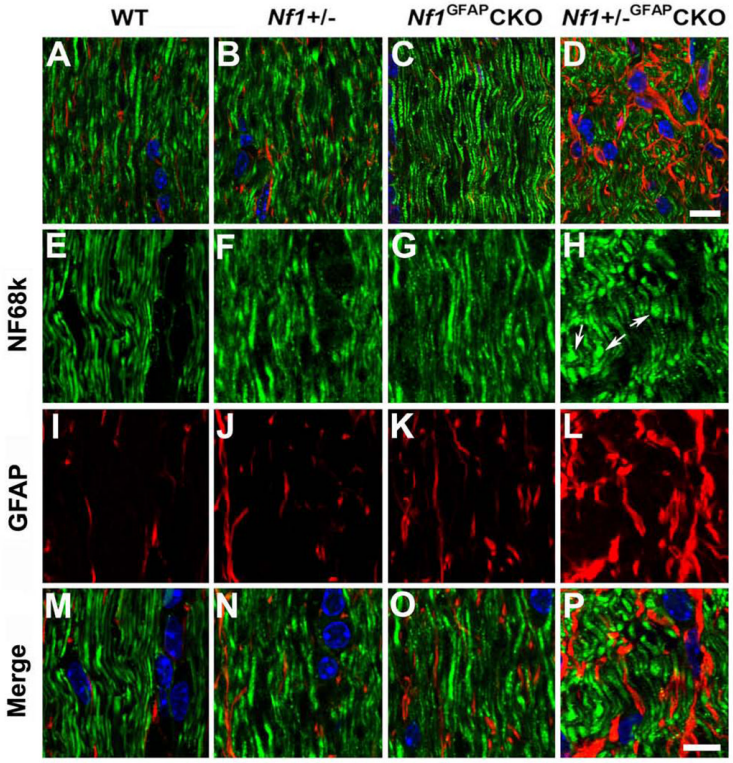

Fig. 4.

Abnormal axon architecture in *Nf1*+/–^{GFAP}CKO mice. Sections from 9-month-old wild-type (A, E, I, M), *Nf1*+/− (B, F, J, N), *Nf1*^{GFAP}CKO (C, G, K, O) and *Nf1*+/–^{GFAP}CKO (D, H, L, P) mice were double labeled with Neurofilament 68k and GFAP antibodies. Well-oriented axonal fiber projections and GFAP-positive astrocytes with elongated processes were present in the pre-chiasmatic optic nerves of wild-type (A, E, M), *Nf1*+/− (B, F, N), and *Nf1*^{GFAP}CKO (C, G, O) mice. In contrast, comparable regions from *Nf1*+/–^{GFAP}CKO mice revealed disoriented axonal fiber projections, and axonal swelling and bulbs (D, H, P), as well as irregularly-shaped and thickened GFAP-positive cells (D, L, P). Scale bars: (A-D) 10 μm; (E-P) 5 μm.

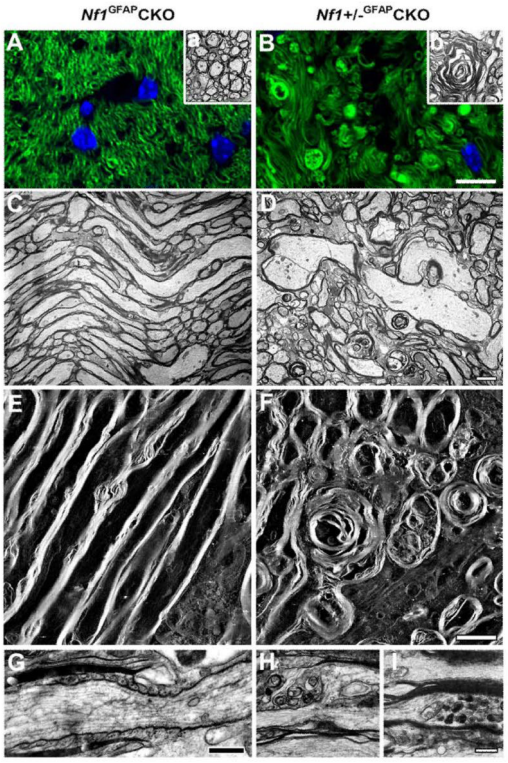

Fig. 5.

Axonal and myelin degeneration in pre-chiasmatic optic nerves of *Nf1*+/–^{GFAP}CKO mice. Cross (A, B) or longitudinal (C-I) sections from 9-month-old *Nf1*^{GFAP}CKO (A, C, E) and *Nf1*+/–^{GFAP}CKO (B, D, F, G) mice were stained with FluoroMyelin (green). The cross section of pre-chiasmatic optic nerves from *Nf1*+/–^{GFAP}CKO mice exhibited the severe alterations such as disruption of the myelin, hypermyelination, spherical lamellar bodies and focal disruption of the axon bundles (B) compared to *Nf1*^{GFAP}CKO mice. EM thin sections (C, D) and 3D projections of EM tomograms (E, F) demonstrate linear optic nerve axon fiber orientation in *Nf1*^{GFAP}CKO 9 month-old mice (C, E). In contrast, comparable regions in *Nf1*+/–^{GFAP}CKO mice showed disorientated fiber projections with degeneration of axonal profiles and myelin (D, F). A representative axon is shown with well developed internodal lamellar spheroids (F). The node and paranode regions in *Nf1*^{GFAP}CKO mice were indistinguishable from wild-type mice (G), whereas the paranode organization was disrupted in *Nf1*+/–^{GFAP}CKO mouse optic nerves. Nodal blebs correlated with the loss of subaxolemmal density (H) and the accumulation of dense bodies within swollen axons (I). Scale bars = (A, B) 10 μm; (C-I) 2μm.

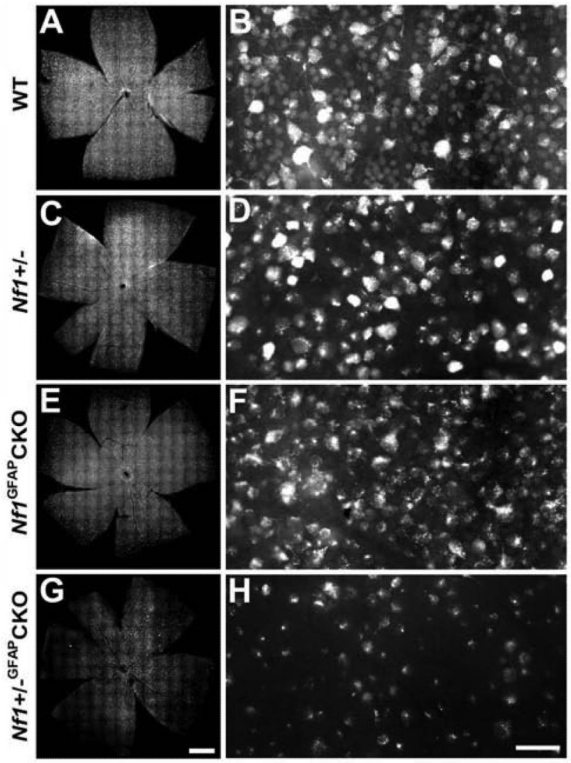

Fig. 6.

RGC neuronal loss in *Nf1*+/–^{GFAP}CKO mice. Representative retinal flat-mounts and sections from 9-month-old wild-type (A, B), *Nf1*+/− (C, D), *Nf1*^{GFAP}CKO (E, F) and *Nf1*+/–^{GFAP}CKO (G, H) mice. Compared to wild-type, *Nf1*+/−, and *Nf1*^{GFAP}CKO mice, *Nf1*+/–^{GFAP}CKO mouse retina showed a significant decrease in the numbers of RGC neurons. Scale bars = (A, C, E, G) 100 μm; (B, D, F, H) 20μm.

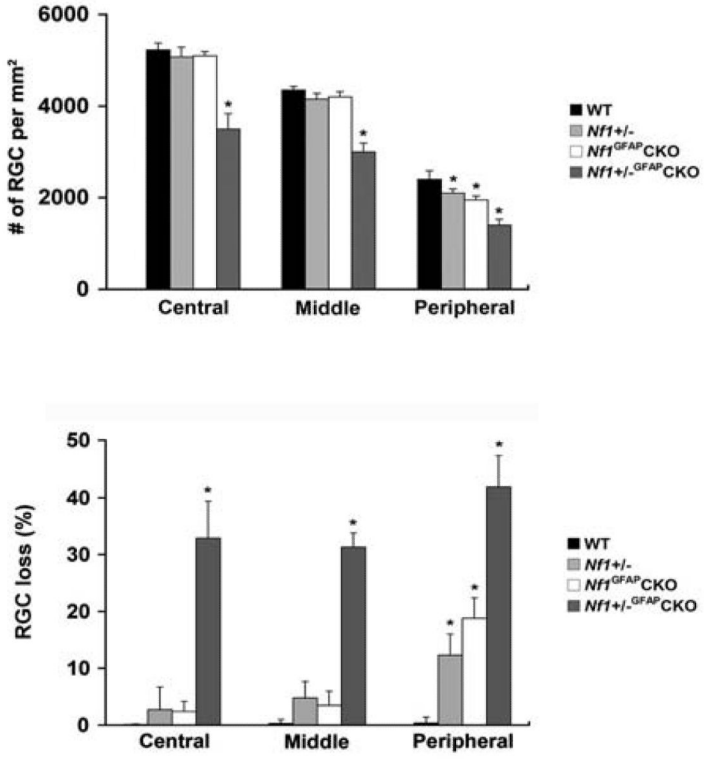

Fig. 7.

Quantification of RGC neuronal loss in *Nf1*+/−^{GFAP}CKO mice. *Nf1*+/−^{GFAP}CKO mice had greater RGC neuron loss compared to wild-type, *Nf1*+/− and *Nf1*^{GFAP}CKO mice. Error bar=SD. **p* < 0.05 compared with wild-type mice, *n* = 4 retinal flat-mounts/mouse/group).

Table 1

RGC neuron densities in 9-month-old *Nf1* mutant mice.

Strain	Age (Months)	RGC neuronal density per retina (RGC neurons/mm^2)		
		Central	Middle	Peripheral
WT	9	5225 ± 156	4350 ± 82	2400 ± 189
Nf1+/−	9	5075 ± 210	4150 ± 130	2100 ± 90*
Nf1^{GFAP}CKO	9	5100 ± 91	4200 ± 113	1950 ± 86*
Nf1+/−^{GFAP}CKO	9	3500 ± 338*	3000 ± 192*	1400 ± 129*

Values are shown as the mean ± SD.

*$P < 0.05$ compared with 9-month-old wild-type mice, $n = 6$ retinal flat-mounts/mouse/group).